Stability of Aβ11–40 Trimers with Parallel and Antiparallel β-Sheet Organizations in a Membrane-Mimicking Environment by Replica Exchange Molecular Dynamics Simulation

Son Tung Ngo, Phuong H. Nguyen, Philippe Derreumaux

Stability of Aβ11-40 Trimers with Parallel and Antiparallel β-Sheet Organizations in a Membrane-Mimicking Environment by Replica Exchange Molecular Dynamics Simulation

Son Tung Ngo,[1,2] Phuong H. Nguyen,[3,4] Philippe Derreumaux,[5,6*]

[1]Laboratory of Theoretical and Computational Biophysics, Ton Duc Thang University, Ho Chi Minh City, Vietnam

[2]Faculty of Applied Sciences, Ton Duc Thang University, Ho Chi Minh City, Vietnam

[3] CNRS, Université de Paris, UPR 9080, Laboratoire de Biochimie Théorique, 13 rue Pierre et Marie Curie, 75005, Paris, France

[4] Institut de Biologie Physico-Chimique-Fondation Edmond de Rothschild, PSL Research University, Paris, France

[5] Laboratory of Theoretical Chemistry, Ton Duc Thang University, Ho Chi Minh City, Vietnam

[6] Faculty of Pharmacy, Ton Duc Thang University, Ho Chi Minh City, Vietnam

ABSTRACT: The aggregation of the Amyloid (Aβ) peptide of 39-43 amino acids into plaques is observed in the brain of Alzheimer's disease (AD) patients, but the mechanisms underlying the neurotoxicity of Aβ oligomers are still elusive. One suggested initial mechanism is related to the implications of amyloid membrane interactions, but characterization of these assemblies is challenging by experimental means. In this study, we have explored the stability of a trimer of Aβ11-40 in parallel and antiparallel β-sheet structures for the wild-type sequence and its F20W mutant in a DPPC membrane using atomistic replica exchange molecular dynamic simulations. We show that both the U-shape organization and the assembly of β-hairpins are maintained in the membrane and are resistant to the mutation F20W. In contrast the models are destabilized by the F19P mutation. Overall, our results indicate that these two assemblies represent minimal seeds or nuclei for the formation of either amyloid fibrils, a variety of β-barrel pores or various aggregates for many Aβ sequences in a membrane-mimicking environment.

INTRODUCTION

Several millions of people are affected by Alzheimer's disease (AD).[1] There is a general consensus that the low molecular weight oligomers of the amyloid-beta (Aβ) peptide consisting of 39-43 amino acids initiate a series of events leading to neuronal death.[2,3] High-resolution knowledge of Aβ oligomers interacting with the membrane is experimentally challenging because these interactions and the oligomer populations are heterogeneous, very dynamic and vary with membrane composition and Aβ amino acid sequence.[4] Amyloid oligomer affinity of Aβ and other amyloid proteins with membrane and their interactions have been explored by a variety of experimental techniques such as transmission electron microscopy (TEM), atomic force microscopy (AFM), nuclear magnetic resonance (NMR), ion mobility – mass spectrometry, small angle neutron scattering, infrared and fluorescence spectroscopies and electric recording.[5-9] From these observations, several Aβ-induced membrane effects have been captured and three generic models have been proposed: the carpeting model with accumulation of amyloid oligomers on membrane surface leading to bilayer deformation, the detergent model where Aβ oligomers have an important detergent-like effects on lipid membrane bilayers and remove lipid molecules from the bilayer, and the amyloid pore hypothesis.[5,10,11]

Among the long list of experimental results, Aβ monomers have much lower membrane affinity than the small oligomers,[12] membrane-bound tetramer and trimer Aβ oligomers correlate with toxicity towards cultured neurons,[13] and a single-molecule study reported that trimers and tetramers may be the smallest Aβ40 oligomers in the anionic lipid bilayers and could be the origin of neurotoxicity.[14]

Carulla et al. reported, based on sodium dodecyl sulfate polyacrylamide gel electrophoresis (SDS-PAGE), electric recording, circular dichroism (CD) and NMR experiments, that Aβ42 tetramers assemble into β-barrels with an inner pore diameter of 0.7 nm in a membrane-mimicking environment, but it is not the case for Aβ40.[15] Recently, ion mobility – mass spectrometry reveals the formation of β-barrel shaped Aβ42 hexamers in a membrane-mimicking environment based on comparing experimental and calculated collision cross-sections, while Aβ40 mostly formed dimers and trimers.[16] Channel-like annular oligomers formed by Aβ peptides were also reported by AFM with inner cavity pores of 2.0-2.5 nm.[17] Very interestingly, the trodusquemine molecule enhances Aβ42 aggregation, but suppresses toxicity by inhibiting Aβ oligomers binding to cell membranes.[18]

Due to the transient character of amyloid oligomers, amyloid membrane interactions either on the surface or inserted into membrane models have motivated the use of computer simulations based on different levels of protein, lipid and solvent representations.[4,19-21] A molecular dynamics (MD) simu-

lation showed that protofibrillar Aβ trimers might be the smallest seeding nucleus on the self-assembled monolayer surfaces.[22] Aβ dimerization on a membrane surface was also investigated by all-atom MD simulations.[23] Based on atomistic MD simulations of dimers and pentamers of Aβ17-42, Jang et al. suggested that a trimer with a strand-turn-strand (U-shaped) fibrillar motif is the minimal oligomer size to insert into the membrane.[24] Brown and Bevan performed MD simulations of Aβ42 tetramer in the presence of a pure POPC or cholesterol-rich raft model membrane and observed the formation of rod-like structures.[25] Feng et al. carried out atomistic MD simulations of Aβ42 dimers differing in the orientation of the two peptides to study the structural stability and damaging effect on a DPPC membrane, they suggested one stable dimeric unit.[26] Strodel and Wales used basin-hopping global optimization tempering and an oligomer generation procedure to identify the most stable structures for the Aβ42 peptide monomer and oligomers (up to octamer) inserted into an implicit lipid bilayer.[27] Of particular interest is that the most stable conformation of the monomer embedded in the implicit membrane displays the U-shaped motif observed in synthetic Aβ40 amyloid fibrils in vitro, and they proposed Aβ42 pore models composed of tetramer to decamer subunits. Atomistic MD and potential of mean force simulations reported that Aβ11–42 peptide oligomers larger than dimers are more likely to lead to lipid deformation and water channels in a POPC membrane.[28]

Recently, we designed atomic structures of β-barrel Aβ40 and Aβ42 tetramers in a membrane model.[29] These models consist of four β-hairpins spanning approximately residues 14-35; this hairpin has already been discussed with a non-negligible probability by dimer simulations of Aβ40 and Aβ42 peptides,[30-32] and Aβ fragments [33,34] in aqueous solution. Using extensive replica exchange molecular dynamics (REMD) simulations, the tetrameric β-barrel made of two distinct β-hairpins is drastically destabilized for Aβ40 with respect to Aβ42 in a bilayer mimicking a neuronal membrane.[29] As β-barrels consisting of one layer of strands have been evidenced by X-ray micro-crystallography for an 11-residue peptide[35] and by simulations for various short-amyloid peptides using multiple representations and sampling techniques in aqueous solution,[36-40] we found using enhanced sampling and the CHARMM-M36m-TIP3P force field designed for intrinsically disordered proteins[41] that Aβ42 barrel tetramer, but not its Aβ40 counterpart, is likely to exist in aqueous solution.[42]

In the present study, based on previous experimental and theoretical results on other systems, namely the co-existence of multiple intramolecular structures, we have tested by enhanced sampling simulations whether Aβ trimers with U-shape (fibril-like) conformations or resulting from hairpin assembly are likely states for the wild-type sequence embedded in a membrane. We emphasize that folding and self-assembly of a trimer of Aβ from randomly chosen conformations in a membrane are not

attainable at an atomistic level, free of any collective variables.[19,43] To further reduce the computer time, the N-terminus (residues 1-10) is excluded as this region is evidenced to be disordered in a membrane-mimicking environment,[15] and the N-truncated Aβ9-42 peptide forms toxic ion channel in the lipid bilayers.[44]

MD and REMD simulations are ideal tools to examine the impact of specific mutations on the conformational ensemble of Aβ peptides. We demonstrated by atomistic REMD simulations that A2V and A2T mutations drastically change the conformational ensemble of Aβ monomer and dimer in aqueous solution.[45-47] Nussinov and coworkers have determined by MD simulations the impact of single mutations and N-terminally modified truncated Aβ variants on the stability of double-sheets pores in membranes.[8,44] In this work, we have examined the effect of the mutations F20W and F19P. This choice is motived by the fact that these mutations are located in the central hydrophobic core (CHC) spanning residues 17-21, recognized as driving Aβ β-sheet and amyloid fibril formation.[4] The substituted tryptophan at amyloid-Aβ residue 20 experiences different environments after fibril formation compared to the WT sequence in vitro, but both WT and F20W peptides display similar aggregation kinetics.[48] In contrast, the F19P mutation forms small Aβ aggregates and prevents the formation of the nucleus and therefore blocks fibril formation in vitro.[49,50] By using MD simulations, Nussinov et al. found that F19P destabilizes the pore ability of Aβ17-42 and Aβ42 peptides, pores consisting of annular U-shaped β-sheets, and this mutation prevents ions permeating across the bilayer.[44]

Here, through the application of REMD simulations to Aβ11-40 WT and its F20W mutant starting from our two β-sheet organizations, and MD simulations with WT and F19P sequences, we can validate our models and determine their robustness.

MATERIALS AND METHODS

Initial structures of the parallel and antiparallel β-sheets

The parallel (P) Aβ11-40 trimer with U-shaped conformations was extracted from the Aβ11-40 amyloid fibril structure.[51] The antiparallel (AP) trimer with β-hairpin conformations was extracted from our Aβ beta-barrel[29] by deleting the hairpin 4; that is our barrel consists of the assembly of two types of hairpins (hairpin 1 and hairpins 2/3 having different intramolecular structures). All peptides were substituted at position 20 by a tryptophan or at position 19 by a proline using PyMOL tool.[52]

The (x, y, z) dimensions of the lipid bilayers are: 6.418 x 6.444 x 4.00 nm for the parallel Aβ β-sheet model and 6.766 x 6.792 x 4.00 nm for the antiparallel Aβ model. All systems were solvated by a 3-particle water model. The parallel F20W trimer is centered in a rectangular box of

$6.418 \times 6.444 \times 7.597$ nm and consists of 125 DPPC molecules, 3923 water molecules, 3 Na^+ ions for a total number of 16,987 atoms vs. 16,975 atoms for its parallel WT counterpart. The anti-parallel F20W and WT systems are centered into a rectangular box of $6.766 \times 6.792 \times 7.097$ nm. The AP F20W system comprises 124 DPPC molecules, 3736 water molecules, and 3 Na^+ atoms for a total of 18,296 atoms, vs. 18,284 for the AP WT system. The initial AP and P trimer structures are shown in Figure 1.

REMD and MD simulations

REMD simulations were carried out using GROMACS version 5.1.3,[53] the united-atom force field GROMOS 53a6[54] for the peptides, the Berger force field[55] for the DPPC lipid bilayer and the SPC water model.[56] The peptides at pH 7 have NH_3^+ and CO_2^- termini, deprotonated Glu and Asp, protonated Arg and Lys, and neutral His with a protonated Nepsilon atom. Following earlier computational studies, simulations were performed with periodic boundary conditions, a time step of 2 fs using LINCS, the velocity Verlet integrator, the Nose-Hoover thermostat, electrostatic interactions were calculated using the particle mesh Ewald (PME) method and a cut-off of 0.9 nm, and Van der Waals interactions used a cut-off of 0.9 nm.[57,58] Starting from the initial conformation, each system was minimized using steepest descent method using weak backbone constraints followed by 500 ps of NVT simulations with a weak harmonic force on the protein atom positions and the system was further relaxed by 1 ns free of any restraints at 324 K. Each relaxed system was then subject to REMD. Parallel F20W Aβ11-40 trimer was investigated using 32 replicas ranging from 321 to 423 K, each replica for 350 ns, as for the parallel WT Aβ11-40 trimer.[58] The antiparallel WT and F20W Aβ11-40 trimers used 28 replicas between 321 and 408 K, each replica for 350 ns. Temperature values for the replicas are given in Supplementary Information (SI). Exchanges between replicas were attempted every 1ps.

The two β-sheet organizations were also subject to MD simulations of 250 ns at 324 K with the WT and F19P sequences starting from the most stable predicted REMD conformations of the WT sequence. In these simulations, we used the CHARMM36m force field for the proteins and lipids, and the modified TIP3P force field for water.[41]

Analysis

An intermolecular and intramolecular side-chain contact is defined when the smallest distance between two side-chain residues of any chains is shorter than 0.45 nm. The hydrogen bond is considered formed when the distance between the donor and the acceptor is shorter than 0.35 nm, and the angle of donor - hydrogen – acceptor is larger than 135^0. A side chain salt-bridge is defined when the distance between two charged groups is smaller than 0.46 nm. The radius of gyration (Rg) is computed

with GROMACS tools. The secondary structure compositions are calculated using DSSP package.[59] The collision cross section (CCS) of each system is calculated using the trajectory method of the IMPACT program.[60] The free energy landscape is constructed using GROMACS tool "sham" projected on the backbone root-mean-square deviation (RMSD) using the full sequences and the number of intermolecular side-chain contacts (SC). The lipid order parameters were calculated using the formula:

$$S_{CD} = \frac{1}{2} 3cos^{\bar{2}}\theta - 1$$

where C is carbon, D is deuterium, and θ is the MD/REMD-averaged angle between the molecular axis given by C_{i-1} - C_{i+1} vector and the bilayer normal.

RESULTS AND DISCUSSION

REMD simulation convergence and data analysis of the parallel WT trimer at 324 K have already been described in Ref. 58; 324 K is selected because membrane DPPC lipid bilayers have a phase transition at 315 K. For the three new REMD simulations, the average of exchange rates between neighboring replicas is on the order of 21% (Figure S1) and there is a satisfactory propagation of the 1st (black) and last (28th or 32th in red) replicas over the temperature range (Figure S2). The convergence of each new simulation at 324 K is demonstrated by the nice overlap of the distributions of the four RMSD, Rg, CCS and β-sheet metrics using the intervals 200-280 ns and 200-350 ns (Figures S3-S5).

There are clear differences in the distributions between the four systems at 324 K. Upon F20W mutation, the mean Rg value increases from 1.42 ± 0.02 to 1.49 ± 0.02 nm in the parallel organization, but remains constant in the antiparallel organization (1.47 ± 0.02 nm for WT, 1.44 ± 0.04 nm for F20W). This conformational change in the parallel architecture is further illustrated by the mean CCS values ranging from 13.42 ± 0.31 nm^2 in WT vs. 14.19 ± 0.31 nm^2 in F20W. In contrast, the averaged CCS values remain centered at 14.35 ± 0.40 nm^2 for WT and F20W in the antiparallel architecture.

In the parallel structure, the β-sheet content changes upon F20W mutation increasing from 40 ± 7% in WT to 47 ± 4%, accompanied by a reduced coil content of 51 ± 4% in F20W vs. 57 ± 7% in WT. The β-sheet content is higher in antiparallel structure, independently of the sequence, that is 50 ± 6% for WT and 52 ± 5% for F20W, with a coil content amounting to 48 ± 7% in WT and 45 ± 6% in F20W. The propensity to form specific secondary structures along each amino acid averaged over the three chains is shown in Figure 2 for the four systems. The results reveal that in the parallel organization the F20W mutation increases mainly the β-strand percentage of the CHC region and residue 30, while the coil and turn contents remain relatively unmodified. In the antiparallel organization, the secondary structure profiles of the WT and F20W peptides superpose relatively well, except the turn content of

residues 25-26 (increase from 15% in WT to 30% in F20W) and the coil content of residues 24-28 (decrease of 10% from WT to F20W). Note that in all systems, the alpha-helix content is 0% and the turn content is 2-3%.

To investigate how the F20W mutation impacts the conformational ensemble, we looked at side-chain and H-bond contact maps, and found that the maps change little upon mutation starting either from the parallel or the antiparallel configurations (data not shown). Table 1 lists the mean number and standard deviation of the total number of intramolecular and intermolecular for the side chain and H-bond contacts in the four systems. The values of the four metrics do not change from WT to F20W in the antiparallel structure. It is found however that the mean value of intramolecular H-bonds is reduced by 50% from WT to F20W in the parallel structure. Variation is also observed for the percentage of the intramolecular salt-bridge D23-K28 formed varying from 30% (WT) to 2% (F20W) in the parallel configuration and from 6% (WT) to 16% (F20W) in the antiparallel configuration, but not for the intermolecular salt-bridges K16-D23 and K16-D22 (Table 2).

A clustering analysis was performed using a backbone RMSD cutoff of 0.3 nm using the full sequences. The number of clusters is reduced from 25 to 8 upon F20W mutation starting from the parallel β-sheet configuration, and from 13 to 8 upon F20W mutation starting from the antiparallel sheet configuration, indicating that the F20W mutation confers less conformational freedom of the Aβ peptides in the membrane. Figures 3 and 4 show the free energy landscape of the four systems projected on the backbone RMSD and the number of intermolecular side-chain contacts, along with the representative structure of each significant free energy minimum. The structural characteristics of these minima are described in Table 3.

For the trimers in parallel structure (Figure 3), we find seven dominant states for the WT sequence designated as WP1-WP7 with populations varying between 19% (WP4) and 6% (WP1). All seven minima totaling 66% of the full conformational space preserve the U-shaped conformations with a rather constant CCS value (13.2 – 13.8 nm^2) and a β-sheet content varying between 56 (WP2) and 34 (WP1) %. The minima differ, however, in their positions within the membrane and the residues located in the extracellular part: residues 11-13 and 25-28 (WP2, WP4, WP5 and WP7 for a population of 42%) or the same previous residues with the N-terminal hydrophobic residues 39 and 40 (WP1, WP3 and WP6 for a population of 22%). Upon F20W mutation, there are five dominant states representing 79% of the full conformational space, with MP3 (44%), MP1 (16%) and MP4 (13%), representing a population of 73%, that have high β-sheet content (46-54%), and CCS values varying between 13.4 (MP3) and 15.1 (MP1) nm^2. Overall, compared to the WT sequence, the F20W mutation increases the β-sheet content, the

CCS value of some minima and the number of conformations with the residue 40 in the extracellular part (63%), but does not impact the fluidity of the membrane (see Figure S6).

It is interesting that the Aβ11-40 trimer with fibrillar conformation remains stable in the membrane. This finding further supports previous MD simulations, having much less sampling capabilities than our REMD, proposing that the Aβ17-42 trimer with a strand-turn-strand (U-shaped) fibrillar motif is the minimal oligomer size to insert into a DOPC membrane.[24] Taken with the MD simulation results of Aβ17-42 dimer,[24] our REMD simulation results in a DPPC membrane strongly suggest that the trimer in parallel structure might be a nucleus for larger cross-β aggregates within the membrane. Our finding that the F20W mutation slightly modifies the free energy landscape of the WT sequence, although inducing change in local flexibility and reducing heterogeneity of the conformation ensemble, is reminiscent of Aβ40 F20W aggregation kinetics in aqueous solution that reported a difference in the inner core and homogeneity of the fibril.[48] Of interest also is that the impact of F20W mutation is much less severe than the A21G mutation, known to lead to early-onset AD,[4] which was found on the same system to destabilize much more the U-shaped conformation.[61]

Next we characterized the trimers in antiparallel structure (Figure 4). For the WT sequence, we find five dominant states designated as WA1-WA5 with three states of equal population (23%). Upon F20W mutation, there are two states MA1-MA2 of equal population (47%). Although the seven states differ in terms of CCS, Rg, CCS, RMSD, number of intermolecular side-chain contacts, location of β-strands, they all display at a coarse-grained level the same generic topology, that is a four-stranded β-sheet made of two well-defined β-hairpins stabilized and recovered in part by the third hairpin. While in WT sequence, the N- and C-terminus of the third β-hairpin are well aligned with the four strands β-sheet; this hairpin kinks at residues 17, 18 and 33, and becomes perpendicular to the four-stranded β-sheet. Although the MA1 and MA2 structures are globally very similar, the β-strands in the four strands β-sheet span residues 16-23 and 29-36 (hairpin 1 in grey) and residues 14-22 and 27-34 (hairpin 1 in red) in MA1, and residues 16-22 and 31-38 (hairpin 1 in grey) and residues 13-22 and 26-35 (hairpin 2 in red) in MA1. Also, the loop of the third hairpin consists of residues 25-28 in MA1 and residues 24-29 in MA2; and there are side chain interactions between the CHC of the third hairpin and residues 31 and 32 of the second hairpin (in grey) in MA1 or residues 20, 31 and 35 of the second hairpin in MA2.

Upon F20 W mutation, the third hairpin is misaligned and more disordered with a significant increase of the loop region. The hairpin 3 consists of β-strands spanning residues 16-22 and 31-37 and a loop

spanning residues 23-29 in MA1, residues 14-21 and 30-39 (strands) and 22-27 (loop) in WA2, residues 18-20 and 32-35 (strands) and 22-30 (loop) in MA3 and residues 14-22, 31-39 (strands) and 23-30 (loop) in WA4. As a consequence of these conformational differences, the number of extracellular residues varies mutation, with the N-terminus (residues 11-14) and loop region (residues 23-27) for the WT sequence, and the more of less same N-terminus and loop region residues along with the two C-terminus residues for the F20W sequence. As for the trimer in parallel structure, the trimer in antiparallel structure for the WT and F20W sequence does not impact the lipid order parameters of the membrane (Figure S6).

It is interesting that at least two well-packed and formed β-hairpins stabilized by a more disordered hairpin remain formed inserted into the membrane for the WT and F20W sequences. These two hairpins have however distinct intramolecular conformations, spanning for example residues 16-38 and 13-35, and differ therefore from the hairpin spanning residues 17-36 proposed by Strodel and Wales,[27] and Graslund et al.[16] This finding makes it clear that this trimer represent a stable seed for creating a large variety of pores made of a single wall (single layer) of β-hairpins (4-mers, 6-mers and 12-mers) within the membrane.

It is important to determine to what extent our results depend on other mutations and the force field. To this end, we performed MD simulations of the WT and F19P trimers with the charmm36m/TIP3P-modified force field starting from the most populated REMD structures from the two WT systems: WP4 (for the parallel structure) and WA4 (for the antiparallel structure). Our total MD trajectory of 1 microsecond at 324K for the four systems makes it clear that both WT trimers deviates little from their initial structures with a plateau at a RMSD of 0.30 nm from 100 to 250 ns, see (A) and (C) in Figure 5. In contrast, the F19P mutation induces much larger RMSD deviation at 250 ns: about 0.55-0.6 nm for F19P in parallel and antiparallel structures, see (B) and (D) in Figure 5. Figure 6 shows the representative structures of the 4 systems based on cluster analysis of the trajectories between 230 and 250 ns. The results on the WT sequence are similar between the GROMOS53a6/Berger/SPC and the CHARM-M36m/TIP3P-modified force fields, small RMSD differences and differences of 7% of β-sheet content. The result of our F19P simulation starting from a U-shaped conformation helps understand why the impact of F19P substitution induces a collapse of the Aβ17-42 and Aβ42 pores.[44] The result of our F19P simulation starting from three β-hairpins shows a clear trend, although the simulations have certainly not reached equilibrium, that is the F19P substitution clearly changes the packing and orientation of the hairpin assembly.

CONCLUSION

In summary, based on extensive REMD simulations on the WT and F20 Aβ11-40 trimer with GROMOS53a6/Berger/SPC force field, and MD simulations on the WT trimer with CHARMM36m/ TIP3P-modified force field, we have demonstrated that the trimer of Aβ11-40 can coexist in a U-shape fibrillar organization and an assembly of three distinct β-hairpins in a DPPC membrane. These results indicate that these two trimer assemblies are seeds (or nuclei) for the formation of larger aggregates with fibrillar conformations, and the formation of larger fully closed β-barrels. Based on previous experimental[15,16,62] and theoretical observations,[29] that is Aβ42 has a much higher propensity for amyloid pore than Aβ40, we can clearly assume that our two trimeric β-sheet assemblies will be more stable for Aβ11-42 than Aβ11-40. In contrast, our simulations show that the two models are destabilized by the F19P mutation. he authors use the U-shape fibril structure as starting model for the trimer. Given the fact that there are more recent AB42 fibril structures resolved, such as the S-shape fibril by the Ishii or Linse groups, I am wondering if these conformations could also lead to a similar behavior (ref to be given).

β-barrels made of amyloid peptides can form under various conditions, in aqueous solution,[35] in a membrane,[15,16] and on the surface of carbon nanotubes.[63] It is remarkable that the β-hairpin propensity of amyloid peptides has been evidenced by solution-phase NMR of Aβ, alpha-synuclein, IAPP-affibody complexes, and triangular forms of β-hairpins and their packing to form hexamers and dodecamers have been observed by X-ray crystallography of macrocyclic β-hairpins in aqueous solution.[64] Whether these triangular assemblies can form in membranes remain to be determined. Also it is of interest to determine the effect of membrane composition such as cholesterol, monosialotetrahexosylganglioside (GM1), POPS lipid, and omega3 and omega6 fatty acids,[4,65-67] on the stability of the two β-sheet assemblies with parallel and antiparallel structures.

Finally, because that the amyloid landscape is highly heterogeneous and sensitive to experimental conditions,[44] we cannot neglect that, beyond β-sheet amyloid pores, pores made of helical Aβ peptides may also exist.[7,16,68,69]

ASSOCIATED CONTENT

Supporting Information

Temperatures in REMD simulations. Additional figures S1−S6 report analysis on the three new REMD simulations: the exchange rates between consecutive replicas, the propagation of two replicas over the

temperature index, the distribution of four metrics at two time intervals, and the time-averaged of the lipid order parameters. The material is available free of charge via the Internet at http://pubs.acs.org.

AUTHOR INFORMATION

Corresponding Author

*E-mail: philippe.derreumaux@tdtu.edu.vn.

ORCID

Son Tung Ngo: 0000-0003-1034-1768

Phuong H. Nguyen: 0000-0003-1284-967X

Philippe Derreumaux: 0000-0001-9110-5585

Notes

The authors declare no competing financial interest.

ACKNOWLEDGMENTS

We thank the support of the Vietnam National Foundation for Science & Technology Development (NAFOSTED) under the grant number 104.99-2019.57, University of Paris, and the French State (Grant "DYNAMO", ANR-11-LABX-0011-01, and "CACSICE", ANR-11-EQPX-0008)

REFERENCES

(1) Querfurth, H. W.; LaFerla, F. M., Alzheimer's Disease. N. Engl. J. Med. 2010, 362, 329-344.

(2) Selkoe, D. G.; Hardy, J. The Amyloid Hypothesis of Alzheimer's Disease at 25 Years. EMBO Mol. Med. 2016, 8, 595-608.

(3) Doig, A. J. ; Del Castillo-Frias, M.P. ; Berthoumieu, O. ; Tarus, B. ; Nasica-Labouze, J. ; Sterpone, F. ; Nguyen P.H. ; Hooper, N.M. ; Faller, P. ; Derreumaux, P. Why Is Research on Amyloid-β Failing to Give New Drugs for Alzheimer's Disease? ACS Chem Neurosci. 2017, 8, 1435-1437.

(4) Nasica-Labouze, J.; Nguyen, P.H.; Sterpone, F.; Berthoumieu, O.; Buchete, N.V.; Coté, S.; De Simone, A.; Doig, A.J.; Faller, P.; Garcia, A. et al. Amyloid beta Protein and Alzheimer's Disease: When Computer Simulations Complement Experimental Studies. Chem Rev. 2015, 115, 3518–3563.

(5) Kayed, R. ; Sokolov, Y. ; Edmonds, B. ; McIntire, T.M. ; Milton, S.C. ; Hall, J.E. ; Glabe, C.G. Permeabilization of Lipid Bi-layers is a Common Conformation-Dependent Activity of Soluble Amyloid Oligomers in Protein Misfolding Diseases. J Biol Chem. 2004, 279, 46363-46366.

(6) Liu, L. ; Komatsu, H. ; Murray, I.V. ; Axelsen, P.H. Promotion of Amyloid Beta Protein Misfolding and Fibrillogenesis by a Lipid Oxidation Product. J Mol Biol. 2008, 377, 1236-1250.

(7) Arispe, N. ; Pollard, H.B. ; Rojas, E. Giant Multivelel Cation Channels Formed by Alzheimer Disease Amyloid beta-protein (Abeta P-(1-40)) in Bilayer Membranes. Proc Natl Acad Sci U S A. 1993, 90, 10573-10577.

(8) Gillman, A.L. ; Jang, H. ; Lee, J. ; Ramachandran, S. ; Kagan, B.L. ; Nussinov, R. ; Teran Arce, F. Activity and Architecture of Pyroglutamate-Modified Amyloid-β (AβpE3-42) Pores. J Phys Chem B. 2014, 118, 7335-7344.

(9) Fusco, G. ; Chen, S.W. ; Williamson, P.T.F. ; Cascella, R. ; Perni, M. ; Jarvis, J.A. ; Cecchi, C. ; Vendruscolo, M. ; Chiti, F. ; Cremades, N. et al. Structural Basis of Membrane Disruption and Cellular Toxicity by α-Synuclein Oligomers. Science 2017, 358, 1440-1443.

(10) Berthelot, K. ; Cullin, C. ; Lecomte, S. What Does Make an Amyloid Toxic: Morphology, Structure or Interaction with Membrane? Biochimie 2013, 95, 12-19.

(11) Bode, D.C. ; Freeley, M. ; Nield, J. ; Palma, M. ; Viles, J.H. Amyloid-β Oligomers Have a Profound Detergent-like Effect on Lipid Membrane Bilayers, Imaged by Atomic Force and Electron Microscopy. J Biol Chem. 2019, 294, 7566-7572.

(12) Sarkar, B. ; Das, A.K. ; Maiti. S. Thermodynamically Stable Amyloid-β Monomers Have Much Lower Membrane Affinity Than the Small Oligomers. Front Physiol. 2013, 4, 84.

(13) Jana, M.K. ; Cappai, R. ; Pham, C.L. ; Ciccotosto, G.D. Membrane-bound Tetramer and Trimer Aβ Oligomeric Species Correlate with Toxicity towards Cultured Neurons. J Neurochem. 2016, 136, 594-608.

(14) Ding, H. ; Schauerte, J.A. ; Steel, D.G. ; Gafni, A. β-Amyloid (1-40) Peptide Interactions with Supported Phospholipid Membranes: A Single-molecule Study. Biophys J. 2012, 103, 1500-1509.

(15) Serra-Batiste, M.; Ninot-Pedrosa, M.; Bayoumi, M.; Gairí, M.; Maglia, G.; Carulla, N. Aβ42 Assembles into Specific β-Barrel Pore-Forming Oligomers in Membrane-Mimicking Environments. Proc. Natl. Acad. Sci. U. S. A. 2016, 113, 10866–10871.

(16) Österlund, N. ; Moons, R. ; Ilag, L.L. ; Sobott, F. ; Gräslund, A. Native Ion Mobility-Mass Spectrometry Reveals the Formation of β-Barrel Shaped Amyloid-β Hexamers in a Membrane-Mimicking Environment. J Am Chem Soc. 2019, 141, 10440-10450.

(17) Lashuel, H.A. ; Hartley, D. ; Petre, B.M. ; Walz, T. ; Lansbury, P.T. Jr. Neurodegenerative Disease: Amyloid Pores from Pathogenic Mutations. Nature. 2002, 418, 291.

(18) Limbocker, R. ; Chia, S. ; Ruggeri, F.S. ; Perni, M. ; Cascella, R. ; Heller, G.T. ; Meisl, G. ; Mannini, B. ; Habchi, J. ; Michaels, T.C.T. et al. Trodusquemine Enhances $A\beta_{42}$ Aggregation but Suppresses Its Toxicity by Displacing Oligomers from Cell Membranes. Nat Commun. 2019, 10, 225.

(19) Sahoo, A. ; Matysiak, S. Computational Insights into Lipid Assisted Peptide Misfolding and Aggregation in Neurodegeneration. Phys Chem Chem Phys. 2019, 21, 22679-22694.

(20) Zhang, M.; Ren, B.; Chen, H.; Sun, Y.; Ma, J.; Jiang, B.; Zheng, J. Molecular Simulations of Amyloid Structures, Toxicity, and Inhibition. Isr. J. Chem. 2017, 7-8, 586-601.

(21) Dong, X. ; Sun, Y. ; Wei, G. ; Nussinov, R. ; Ma, B. Binding of Protofibrillar Aβ Trimers to Lipid Bilayer Surface Enhances Aβ Structural Stability and Causes Membrane Thinning. Phys Chem Chem Phys. 2017, 19, 27556-27569.

(22) Wang, Q. ; Zhao, J. ; Yu, X. ; Zhao, C. ; Li, L. ; Zheng, J. Alzheimer Abeta(1-42) Monomer Adsorbed on The Self-Assembled Monolayers. Langmuir. 2010, 26, 12722-12732.

(23) Davis, C.H.; Berkowitz, M.L. A Molecular Dynamics Study of The Early Stages of Amyloid-beta(1-42) Oligomerization: The Role of Lipid Membranes. Proteins. 2010, 78, 2533-2545.

(24) Jang, H. ; Connelly, L. ; Arce, F.T. ; Ramachandran, S. ; Kagan, B.L. ; Lal, R. ; Nussinov, R. Mechanisms for the Insertion of Toxic, Fibril-like β-Amyloid Oligomers into the Membrane. J Chem Theory Comput. 2013, 9, 822-833.

(25) Brown, A.M. ; Bevan, D.R. Molecular Dynamics Simulations of Amyloid β-Peptide (1-42): Tetramer Formation and Membrane Interactions. Biophys J. 2016, 111, 937-949.

(26) Feng, W. ; Lei, H. ; Si, J. ; Zhang, T. Study of Structural Stability and Damaging Effect on Membrane for four Aβ42 Dimers. PLoS One. 2017, 12, e0179147.

(27) Strodel, B.; Lee, J. W.; Whittleston, C. S.; Wales, D. J. Transmembrane Structures for Ahzeihmer's Abeta(1-42)-oligomers. J Am Chem Soc. 2010, 132, 13300-13312.

(28) Xiang, N. ; Lyu, Y. ; Zhu, X. ; Narsimhan, G. Investigation of the Interaction of Amyloid β Peptide (11-42) Oligomers with a 1-palmitoyl-2-oleoyl-sn-glycero-3-phosphocholine (POPC) Membrane Using Molecular Dynamics Simulation. Phys Chem Chem Phys. 2018, 20, 6817-6829.

(29) Nguyen, P.H. ; Campanera, J.M. ; Ngo, S.T. ; Loquet, A. ; Derreumaux, P. Tetrameric Aβ40 and Aβ42 β-Barrel Structures by Extensive Atomistic Simulations. I. In a Bilayer Mimicking a Neuronal Membrane. J Phys Chem B. 2019,123, 3643-3648.

(30) Tarus, B.; Tran, T.T.; Nasica-Labouze, J.; Sterpone, F. ; Nguyen, P.H.; Derreumaux P. Structures of the Alzheimer's Wild-Type Aβ1-40 Dimer from Atomistic Simulations. J Phys Chem B. 2015, 119, 10478-10487.

(31) Cao, Y.; Jiang, X.; Han, W. Self-Assembly Pathways of β-Sheet-Rich Amyloid-β(1-40) Dimers: Markov State Model Analysis on Millisecond Hybrid-Resolution Simulations. J Chem Theory Comput. 2017, 13, 5731-5744.

(32) Man, V. H.; Nguyen, P. H.; Derreumaux, P. High-Resolution Structures of the Amyloid-β 1–42 Dimers from the Comparison of Four Atomistic Force Fields. J. Phys. Chem. B 2017, 121, 5977–5987.

(33) Chebaro, Y.; Mousseau, N.; Derreumaux, P. Structures and Thermodynamics of Alzheimer's Amyloid-beta Abeta(16-35) Monomer and Dimer by Replica Exchange Molecular Dynamics Simulations: Implication for Full-length Abeta Fibrillation. J Phys Chem B. 2009, 113, 7668-7675.

(34) Chebaro, Y. ; Jiang, P. ; Zang, T. ; Mu, Y. ; Nguyen, P.H. ; Mousseau, N. ; Derreumaux ; P. Structures of Aβ17-42 Trimers in Isolation and with Five Small-Molecule Drugs Using a Hierarchical Computational Procedure. J Phys Chem B. 2012, 116, 8412-8422.

(35) Laganowsky, A.; Liu, C.; Sawaya, M.R.; Whitelegge, J.P.; Park, J.; Zhao, M.; Pensalfini, A.; Soriaga, A.B.; Landau, M.; Teng, P.K. et al. Atomic View of a Toxic Amyloid Small Oligomer. Science 2012, 335, 1228-1231.

(36) Melquiond, A.; Mousseau, N.; Derreumaux, P. Structures of Soluble Amyloid Oligomers from Computer Simulations. Proteins. 2006, 65, 180-91.

(37) Bellesia, G. ; Shea, J-E. Effect of Beta-sheet Propensity on Peptide Aggregation. J. Chem. Phys. 2009, 130, 145103.

(38) De Simone, A. ; Derreumaux, P. Low Molecular Weight Oligomers of Amyloid Peptides Display Beta-barrel Conformations: A Replica Exchange Molecular Dynamics Study in Explicit Solvent. J Chem Phys. 2010, 132, 165103.

(39) Sterpone, F.; Melchionna, S.; Tuffery, P.; Pasquali, S.; Mousseau, N.; Cragnolini, T.; Chebaro, Y.; St-Pierre, J.; Kalimeri, M.; Barducci, A. et al. The OPEP Protein Model: From Single Molecules, Amyloid Formation, Crowding and Hydrodynamics to DNA/RNA Systems. Chem. Soc. Rev. 2014, 43, 4871-4893.

(40) Sun, Y. ; Ge, X. ; Xing, Y. ; Wang, B. ; Ding, F. β-barrel Oligomers as Common Intermediates of Peptides Self-Assembling into Cross-β Aggregates. Sci Rep. 2018, 8, 10353.

(41) Huang, J. ; Rauscher, S. ; Nawrocki, G. ; Ran, T. ; Feig, M. ; de Groot, B.L. ; Grubmüller, H. ; MacKerell, A.D. Jr. CHARMM36m: An Improved Force Field for Folded and Intrinsically Disordered Proteins. Nat Methods. 2017, 14, 71-73.

(42) Nguyen, P.H. ; Campanera, J.M. ; Ngo, S.T. ; Loquet, A. ; Derreumaux, P. Tetrameric Aβ40 and Aβ42 β-Barrel Structures by Extensive Atomistic Simulations. II. In Aqueous Solution. J Phys Chem B. 2019, 123, 6750-6756.

(43) Tuffery, P. ; Derreumaux, P. Flexibility and Binding Affinity in Protein-Ligand, Protein-Protein and Multi-Component Protein Interactions: Limitations of Current Computational Approaches. J R Soc Interface. 2012, 9, 20-33.

(44) Jang, H.; Teran Arce, F.; Ramachandran, S.; Kagan, B. L.; Lal, R.; Nussinov, R. Disordered Amyloidogenic Peptides May Insert into the Membrane and Assemble into Common Cyclic Structural Motifs. Chem. Soc. Rev. 2014, 43, 6750–6764.

(45) Nguyen, P.H. ; Sterpone, F.; Campanera, J.M. ; Nasica-Labouze, J. ; Derreumaux, P. Impact of the A2V Mutation on the Heterozygous and Homozygous Aβ1-40 Dimer Structures from Atomistic Simulations. ACS Chem Neurosci. 2016, 7, 823-832.

(46) Nguyen, P.H. ; Tarus, B. ; Derreumaux, P. Familial Alzheimer A2V Mutation Reduces the Intrinsic Disorder and Completely Changes the Free Energy Landscape of the Aβ1-28 Monomer. J Phys Chem B. 2014, 118, 501-510.

(47) Nguyen, P.H. ; Sterpone, F. ; Pouplana, R. ; Derreumaux, P. ; Campanera, J.M. Dimerization Mechanism of Alzheimer $A\beta_{40}$ Peptides: The High Content of Intrapeptide-Stabilized Conformations in A2V and A2T Heterozygous Dimers Retards Amyloid Fibril Formation. J Phys Chem B. 2016, 120, 12111-12126.

(48) McDonough, R. T.; Paranjape, G.; Gallazzi, F.; Nichols, M. R., Substituted Tryptophans at Amyloid-β(1–40) Residues 19 and 20 Experience Different Environments after Fibril Formation. Arch. Biochem. Biophys. 2011, 514, 27-32.

(49) Bernstein, S.L.; Wyttenbach, T. ; Baumketner, A. Shea, J.E. ; Bitan, G. ; Teplow, D.B. ; Bowers, M.T. Amyloid beta-Protein: Monomer Structure and Early Aggregation States of Abeta42 and its Pro19 Alloform. J Am Chem Soc. 2005, 127, 2075-2084.

(50) Daly, S., Kulesza, A.; Poussigue, F.; Simon, A.L.; Choi, C.M.; Knight, G.; Chirot, F.; MacAleese, L.; Antoine, R. Dugourd, P. Conformational Changes in Amyloid-beta (12-28) Alloforms Studied Using Action-FRET, IMS and Molecular Dynamics Simulations. Chem Sci. 2015, 6, 5040-5047.

(51) Bertini, I.; Gonnelli, L.; Luchinat, C.; Mao, J.; Nesi, A., A New Structural Model of Aβ40 Fibrils. J. Am. Chem. Soc. 2011, 133, 16013-16022.

(52) Schrödinger LLC, P. The PyMOL molecular graphics system, Version 1.3r1; August, 2010.

(53) Abraham, M. J.; Murtola, T.; Schulz, R.; Páll, S.; Smith, J. C.; Hess, B.; Lindahl, E. GROMACS: High Performance Molecular Simulations through Multi-Level Parallelism from Laptops to Supercomputers. SoftwareX 2015, 1–2, 19-25.

(54) Oostenbrink, C.; Villa, A.; Mark, A. E.; Van Gunsteren, W. F. A Biomolecular Force Field Based on the Free Enthalpy of Hydration and Solvation: The GROMOS Force-Field Parameter Sets 53A5 and 53A6. J. Comput. Chem. 2004, 25, 1656-1676.

(55) Berger, O. ; Edholm, O ; Jahnig, F. Molecular Dynamics Simulations of a Fluid Bilayer of Dipalmitoylphosphatidylcholine at Full Hydration, Constant Pressure and Constant Temperature. Biophys J. 1997, 72, 2002-2013.

(56) Berendsen, H. J. C.; Postma, J. P. M.; van Gunsteren, W. F.; Hermans, A. J. Intermolecular Forces. Reidel, Dordrecht: Jerusalem, Israel, 1981.

(57) Ngo, S. T.; Luu, X.-C.; Nguyen, M. T.; Le, C. N.; Vu, V. V. In Silico Studies of Solvated F19W Amyloid β (11-40) Trimer. RSC Adv 2017, 7, 42379-42386.

(58) Ngo, S. T.; Hung, H. M.; Tran, K. N.; Nguyen, M. T. Replica Exchange Molecular Dynamics Study of the Amyloid Beta (11-40) Trimer Penetrating a Membrane. RSC Adv. 2017, 7, 7346-7357.

(59) Touw, W. G.; Baakman, C.; Black, J.; te Beek, T. A. H.; Krieger, E.; Joosten, R. P.; Vriend, G., A Series of PDB-Related Databanks for Everyday Needs. Nucleic Acids Res 2015, 43, D364-D368.

(60) Marklund, Erik G.; Degiacomi, Matteo T.; Robinson, Carol V.; Baldwin, Andrew J.; Benesch, Justin L. P., Collision Cross Sections for Structural Proteomics. Structure 2015, 23, 791-799.

(61) Ngo, S.T. ; Nguyen, M.T ; Nguyen, N.T. ; Vu, V.V. The Effects of A21G Mutation on Transmembrane Amyloid Beta(11-40 Trimer : An In Silico Study. J. Phys. Chem. B 2017, 121, 8467-8474.

(62) Bode, D. C.; Baker, M. D.; Viles, J. H. Ion Channel Formation by Amyloid-β42 Oligomers but Not Amyloid-β40 in Cellular Membranes. J Biol Chem. 2017, 292, 1404-1413.

(63) Fu, Z. ; Luo, Y. ; Derreumaux, P. ; Wei, G. Induced Beta-Barrel Formation of the Alzheimer's Abeta25-35 Oligomers on Carbon Nanotube Surfaces: Implication for Amyloid Fibril Inhibition. Biophys J. 2009, 97, 1795-803.

(64) Kreutzer, A.G. ; Nowick, J.S. Elucidating the Structures of Amyloid Oligomers with Macrocyclic beta-Hairpin peptides : Insights into Alzheimer's Disease and Other Amyloid Diseases. Acc. Chem. Res. 2018, 51, 706-718.

(65) Dominguez, L. ; Foster, L.; Straub, J.E. ; Thirumalai D. Impact of Membrane Lipid Composition on the Structure and Stability of the Transmembrane Domain of Amyloid Precursor Protein. Proc Natl Acad Sci U S A. 2016, 113, E5281-5287.

(66) Owen, M.C. ; Kulig, W. ; Poojari, C.; Rog, T. ; Strodel, B. Physiologically-Relevant Levels of Sphingomyelin, but not GM1, Induces a β-Sheet-Rich Structure in the Amyloid-β(1-42) Monomer. Biochim Biophys Acta Biomembr. 2018 pii: S0005-2736(18)30106-8.

(67) Lu, Y. ; Shi, X.F. ; Nguyen, P.H. ; Sterpone, F. ; Salsbury, F.R. Jr ; Derreumaux, P. Amyloid-β(29-42) Dimeric Conformations in Membranes Rich in Omega-3 and Omega-6 Polyunsaturated Fatty Acids. J Phys Chem B. 2019, 123, 2687-2696.

(68) Ngo, S.T. ; Derreumaux, P. ; Vu, V.V. Probable Transmembrane Amyloid α-Helix Bundles Capable of Conducting Ca^{2+} Ions. J Phys Chem B. 2019, 123, 2645-2653.

(69) Pannuzzo, M. ; Milardi, D. ; Raudino, A. ; Karttunen, M. ; La Rosa, C. Analytical Model and Multiscale Simulations of Aβ Peptide Aggregation in Lipid Membranes: Towards a Unifying Description of Conformational Transitions, Oligomerization and Membrane Damage. Phys Chem Chem Phys. 2013, 15, 8940-8951.

Table 1. The average and standard deviation number of intermolecular and intramolecular HB and SC contacts for the P/AP F20W and WT systems. The results are the number of intermolecular contacts between any two chains and the number of intra-molecular contacts per chain. The values for WT (P) are obtained from Ref. 58.

System	Intra-HB	Intra-SC	Inter-HB	Inter-SC
F20W (P)	6.03 ± 2.25	130.41 ± 8.18	11.23 ± 1.11	42.59 ± 3.31
WT (P)	11.27 ± 2.39	141.36 ± 6.27	10.53 ± 1.65	42.69 ± 4.06
F20W (AP)	15.64 ± 1.66	190.35 ± 4.56	4.06 ± 0.59	30.80 ± 2.28
WT (AP)	14.34 ± 1.98	181.51 ± 7.05	3.89 ± 0.81	30.98 ± 4.40

Table 2. The percentage of intra-/intermolecular D23-K28, K16-D23, and K16-E22 salt bridges (SB) formed in the P/AP WT and F20W and WT trimers. The values for WT (P) are obtained from Ref. 58.

	F20W (P)	WT (P)	F20W (AP)	WT (AP)
Intra-SB D23-K28	2 ± 5	30 ± 10	16 ± 9	6 ± 6
Inter-SB K16-D23	0 ± 0	0 ± 0	0 ± 0	2 ± 2
Inter-SB K16-E22	0 ± 0	0 ± 0	27 ± 6	22 ± 5

Table 3. Structural description of the main free energy minima of the WT and F20W P/AP systems. The F20W states in the parallel structure are denoted by MP1, MP2, MP3, MP4, and MP5, the F20W states in the anti-parallel structure by MA1 and MA2, while the corresponding WT states are WP1, WP2, WP3, WP4, WP5, WP6 in the parallel structure and WP7 and WA1, WA2, WA3, WA4, and WA5 in the antiparallel structure.

Shape	R_g (nm)	CCS (nm²)	β-content (%)	Coil-contact (%)	Turn-content (%)	Population (%)	Extracellular residues
MP1	1.50	14.73	46	52	2	16	12-13 and 27-28
MP2	1.47	13.85	42	58	0	5	11-13, 25-27, and 39-40
MP3	1.47	13.41	54	46	0	44	11-12, 26-28, and 40
MP4	1.51	15.06	46	52	2	13	11-13, 24-27, and 40
MP5	1.46	13.57	44	53	2	4	11-13, 25-27, and 40
MA1	1.43	13.90	60	37	3	47	11-13 and 25-27 of chain B, 23-26 of chain A, 11-14 of chain C
MA2	1.48	14.72	56	39	5	47	11-14 and 25-27 of chain B, 23-26 of chain A, 12-14 of chain C
WP1	1.41	13.84	34	66	0	6	11-13, 25-27, and 39-40
WP2	1.42	13.22	56	44	0	13	11-13 and 25-29
WP3	1.45	13.72	40	57	3	10	11-13, 25-27, and 39-40
WP4	1.43	13.11	46	52	2	19	11-13, and 25-28
WP5	1.43	13.13	47	51	2	7	11-13 and 25-28
WP6	1.42	13.03	54	44	2	6	11-13, 25-28, and 40
WP7	1.46	13.69	46	51	3	10	11-13 and 25-28
WA1	1.43	14.25	50	48	2	3	11-13 and 25-29 of chain B, 23-25 of chain A, 42 of chain B, 11-14 of chain C
WA2	1.45	14.52	57	41	2	22	12-14 and 25-27 of chain B, 23-26 of chain A, 11-14 of chain C,
WA3	1.48	14.90	41	59	0	14	11-14, 25-27 and 39-40 of chain B, 22-24 of chain A, 11-14 of chain C
WA4	1.47	14.24	57	41	2	24	11-14 and 25-27 of chain B, 11-12 and 23-25 of chain A, 11-14 of chain C
WA5	1.50	14.85	52	41	7	23	12-14, 25-28 and 40 of chain B, 23-25 of chain A, 11-15 of chain C, 11-13 of chain A

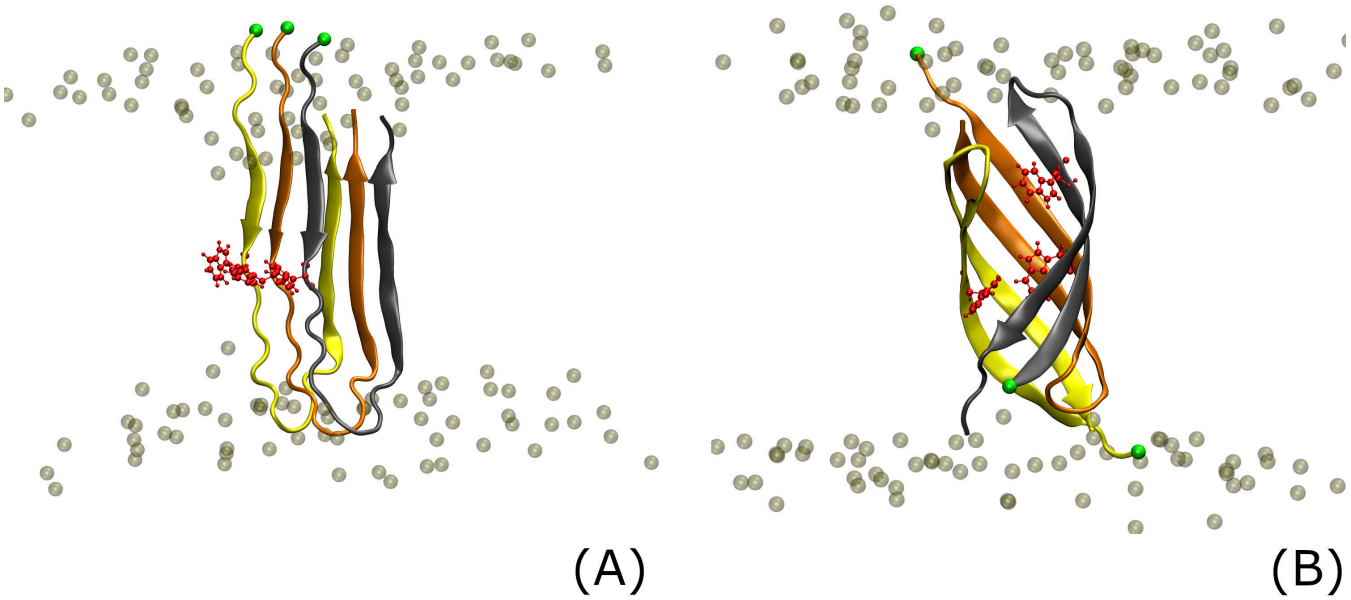

Figure 1. Initial conformations. (A) Parallel F20W trimer with the side-chain atoms of W20 (shown in red); the residues 11-13 and 26-28 are in the extracellular part. (B) Antiparallel F20W trimer with the side-chain atoms of W20 shown in red; the extracellular residues consist of residues 24-25 of chain A, residues 11-14 of chain B, and residues 11-13 of chain; hairpin 1 in chain A is grey, hairpin 2 in chain B is orange and hairpin 3 in chain C is in yellow. C). The green ball denoted the N-terminus of each Aβ11-40 peptide. Tan spheres represent the phosphorus atoms of DPPC membrane. For simplicity, the solvent is not shown.

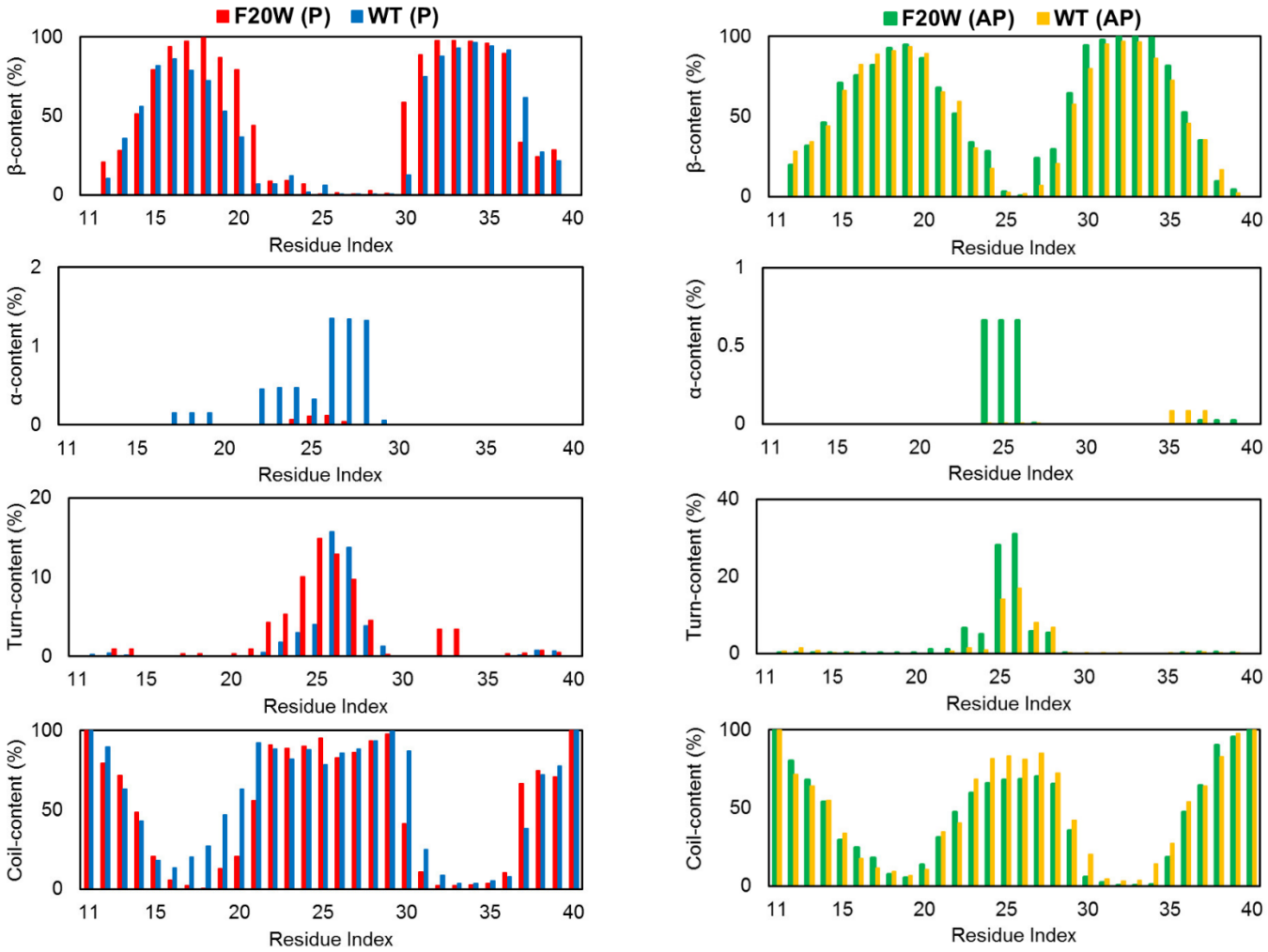

Figure 2. The secondary structure composition along the amino acid sequence for the F20W and WT peptides in parallel (P, left panels) and anti-parallel (AP, right panels) organizations. The metrics of the WT peptide in P structure are taken from Ref. 58.

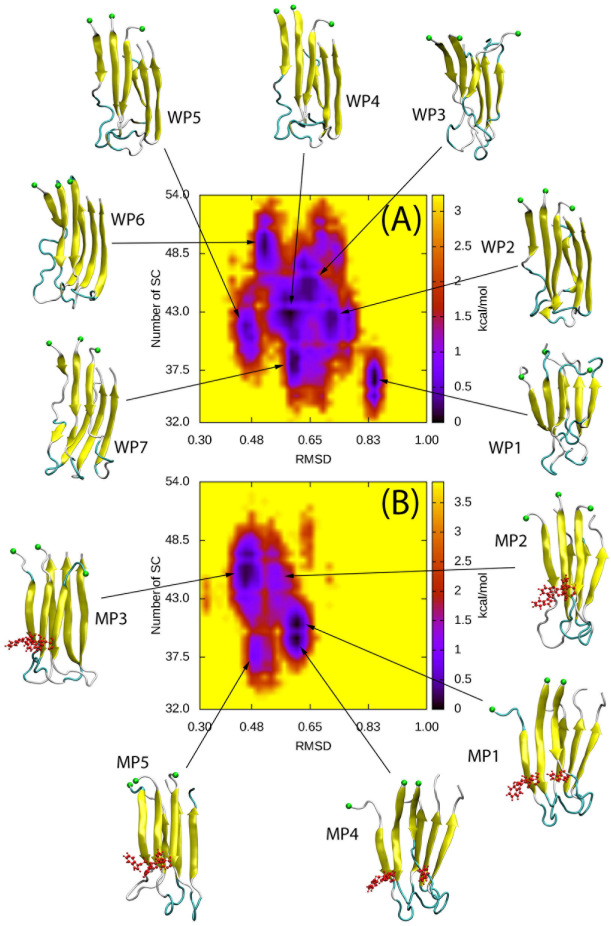

Figure 3. The free energy landscape of the transmembrane Aβ trimers in parallel structure projected on the backbone RMSD and the number of intermolecular SC contacts. (A) WT trimer, in which, the seven main minima WP1-WP7 are located by black arrows at (RMSD; Number of SC) values of (0.83, 36.0), (0.71, 42.1), (0.63, 44.2), (0.59, 43.0), (0.45, 41.8), (0.50, 48.2), and (0.59, 37.5), respectively. (B) F20W trimer with the five main minima MP1-MP5 located at (0.60; 40.2), (0.54; 44.0), (0.45; 45.1), (0.60; 39.0) and (0.48; 37.9).

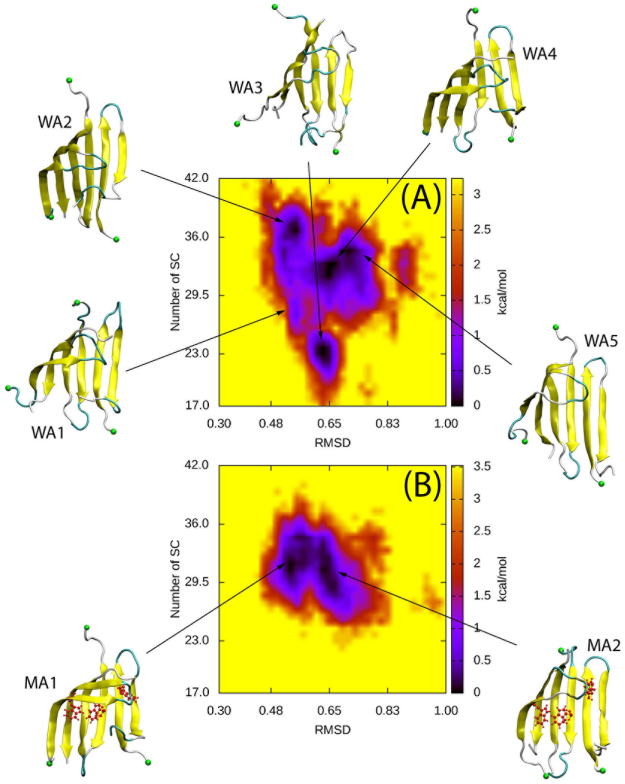

Figure 4. The free energy landscape of the transmembrane Aβ trimers in anti-parallel structure projected on the backbone RMSD and the number of intermolecular SC contacts. (A) The WT system, in which, the main five minima WA1-WA5 are located at (RMSD; Number of SC) values of (0.54; 27.4), (0.54; 36.1), (0.62; 23.2), (0.64; 31.9), and (0.70; 34.0). (B) The F20W system where the main minima MA1 and MA2 are located at (0.53; 31.2) and (0.63; 30.1), respectively.

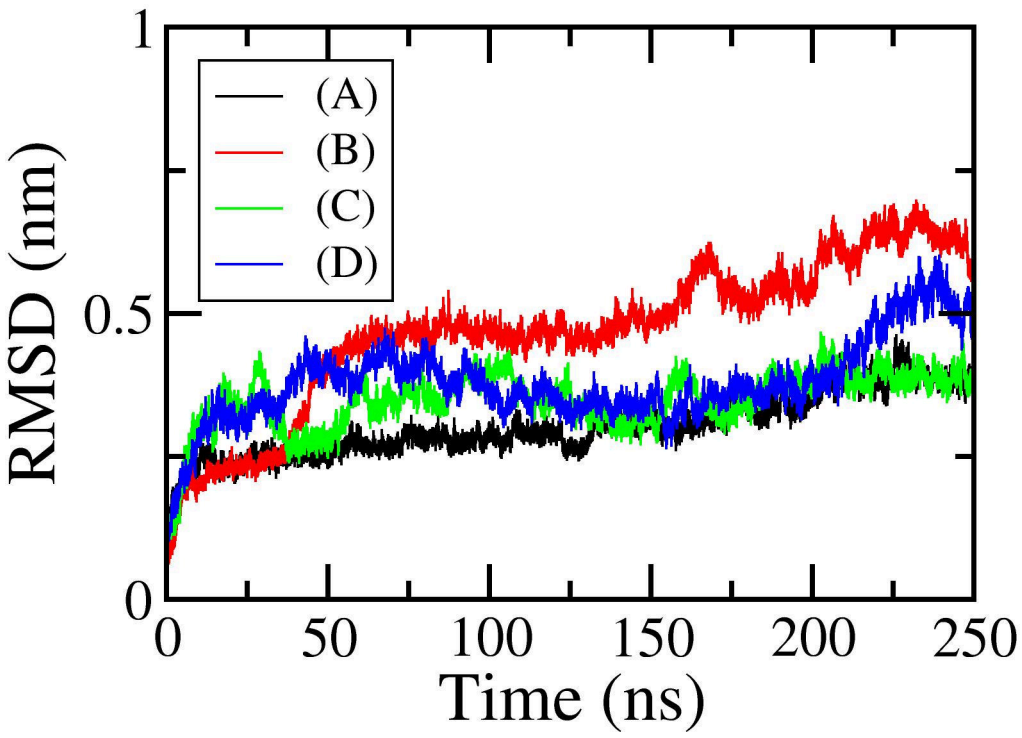

Figure 5. Time evolution of the RMSD of the four systems using CHARM36m/TIP3P-modified force field. (A) refers to WT parallel, (B) to F19P parallel, (C) to WT antiparallel and (D) to F19P antiparallel MD simulations.

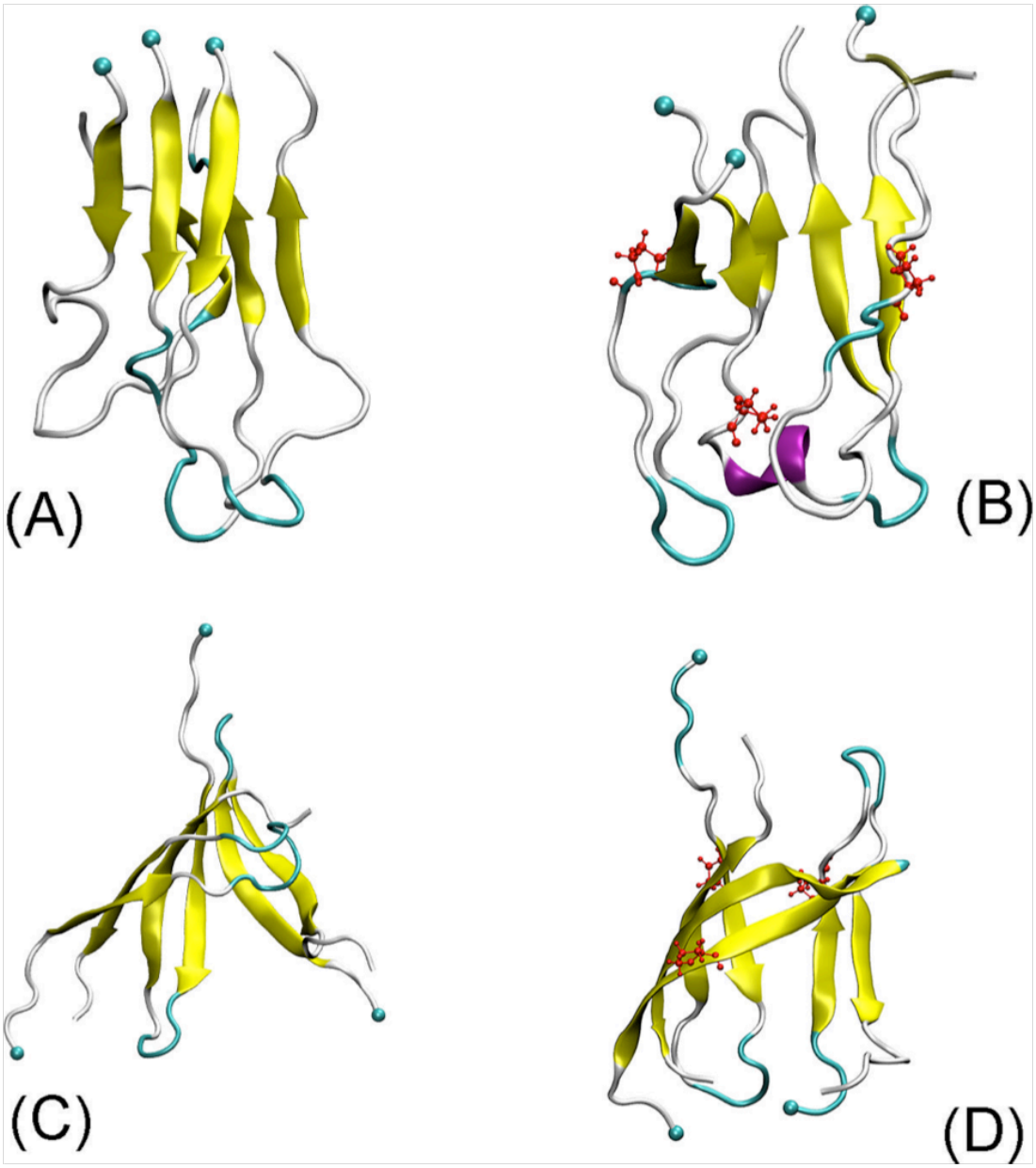

Figure 6. Representative structures of the MD-generated systems using CHARM36m/TIP3P-modified force field. (A) shows the structure for the WT parallel, (B) for the F19P parallel, (C)

for the WT antiparallel and (D) the F19P antiparallel MD simulations using the intervals 230-250 ns. The all-atom proline substitution is shown in (B) and (D).

TOC GRAPHICS